

# Nanoscale

# Friction-reduction effect of the hierarchical surface microstructure of carrion beetle by controlling the real contact area

Journal:	Nanoscale
Manuscript ID	NR-ART-07-2024-002892.R2
Article Type:	Paper
Date Submitted by the Author:	11-Oct-2024
Complete List of Authors:	Tsujioka, Kazuma; Hokkaido University, Graduate School of Chemical Sciences and Engineering Hirai, Yuji; Chitose Institute of Science and Technology, Graduate School of Science and Technology Shimomura, Masatsugu; Chitose Institute of Science and Technology, Graduate School of Science and Technology; Chitose Institute of Science and Technology, Department of Applied Chemistry and Bioscience Matsuo, Yasutaka; Hokkaido University, Research Institute for Electronic Science

SCHOLARONE™ Manuscripts

#### **ARTICLE**

# Friction-reduction effect of the hierarchical surface microstructure of carrion beetle by controlling the real contact area

Kazuma Tsujioka, a Yuji Hirai, b Masatsugu Shimomurab, c and Yasutaka Matsuo\*d

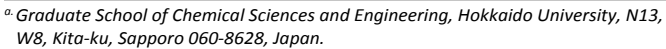
Received 00th January 20xx, Accepted 00th January 20xx

DOI: 10.1039/x0xx000000x

The discovery and elucidation of the surface microstructure functions of living organisms are crucial to resolving issues, such as friction. We newly discovered that Necrophila japonica, a type of carrion beetle that lives on the ground surface, exhibited a hierarchical surface microstructure comprising a submicron-sized wrinkle structure on top of a micron-sized microstructure. The surface microstructure of this beetle improved wettability but did not exhibit superhydrophobicity, a well-known function of hierarchical structures, so it was expected to have a different function. By combining the insights in the field of structural mechanics that avoidance of stress concentration by structural geometry affects deformation with the basic principles of friction, the frictional properties and mechanisms of the hierarchical surface microstructure of the carrion beetle were investigated. The measurements of frictional force indicated that the mimicked structure exerted lower frictional forces than flat and single-layer microstructure surfaces. Analysis of finite element method simulations showed that even though the mimicked structure was prone to pressure concentration due to small contact points, the surface contact pressure was reduced more than that of the single-layer structure by hierarchical load dispersion like that of metamaterials. As a result, the suppression of the increase in real contact area due to deformation suppression contributed to effective friction reduction. The effective friction reduction by hierarchical structure provides new insight into not only the surface microstructure function of organisms, but also the lubricant-free friction reduction that has been the focus of attention in carbon neutrality and other fields.

#### Introduction

Living organisms that have overcome the struggle for survival over a long time sometimes exhibit superior functions through nanometer (nm)— micrometer ( $\mu$ m)-scale surface microstructures <sup>1,2</sup>. For example, the antireflection by the motheye structure observed in the wings of cicadas and the moth eye <sup>3,4</sup>, the adhesion by the hair-like structure with the spatula of geckos and insects <sup>5–7</sup>, and the mucus adhesion-enhancing function by the nanofilaments of abalones and clingfish have been reported <sup>8,9</sup>. The principles of these surface microstructure functions can be applied to various fields by elucidating them, thereby equipping humanity with problem-solving clues. Therefore, learning from organisms, i.e., discovering the surface microstructure functions, elucidating their principles, and applying them to the resolution of human challenges, represents a very crucial research hotspot.



b. Graduate School of Science and Technology, Chitose Institute of Science and Technology (CIST), Bibi 758-65, Chitose, 066-8655, Japan.

Supplementary Information available: [details of any supplementary information available should be included here]. See DOI: 10.1039/x0xx00000x

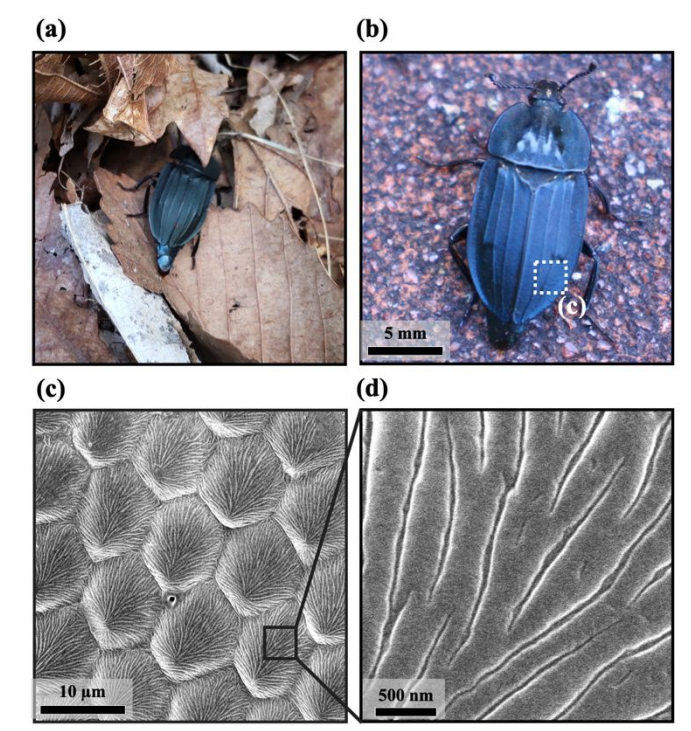


Figure 1 (a, b) Photographs of carrion beetle (*Necrophila japonica*) and (c, d) field emission scanning electron microscope (FE-SEM) images of elytra. In elytra, (c) microstructures of micron order were arranged almost in a hexagonal lattice, and (d) wrinkle structures of submicron order were on the microstructures. Samples were collected in Bibi, Chitose City, Hokkaido, Japan.

C Department of Applied Chemistry and Bioscience, Chitose Institute of Science and Technology (CIST), Bibi758-65, Chitose, 066-8655, Japan.

d. Nanotechnology Research Center, Research Institute for Electronic Science, Hokkaido University, N21W10, Kita-ku, Sapporo, 011- 0021, Japan.
†Kazuma Tsujioka: JSPS Research Fellow (DC2).

We newly discovered that the Necrophila japonica, a type of carrion beetle, exhibits a hierarchical surface microstructure in which a submicron-scale wrinkle structure exists on a microscale microstructure dome (Figure 1). This structure was mainly confirmed on the elytra but not on the back of the elytra (Figure S1). The Necrophila japonica mainly feeds on dominant macroinvertebrates of soil ecosystems and often lives on forest surfaces (beneath fallen leaves, etc.) 10-12 (Figure 1(a)); however, the functions of its hierarchical surface microstructure are unknown. Previous studies revealed that the hierarchical surface microstructure mostly superhydrophobicity functions (self-cleaning of dirt-containing bacteria, ensuring breathing, etc. <sup>13–17</sup>), and famous examples include lotus leaves 14,18,19 and springtails 13,20 that live around forest surfaces, similar to the carrion beetle. However, superhydrophobicity was not observed when we evaluated the wettability of the hierarchical structure of Necrophila japonica (contact angle: ~90°, Figure S2). The wettability of the hierarchical surface microstructure of the slithering gecko (a gecko crawls like snakes as it does not have legs), which exhibits a wrinkled structure on top of a microstructure similar to the Necrophila japonica, has been evaluated, although it also failed to exhibit superhydrophobicity <sup>21</sup>. Conversely, the group that studied slithering geckos suggested, without examining the details, that the hierarchical structure on their dorsal side may have evolved from their contact with leaves and other objects on their backs while crawling and may have exerted some frictional effects <sup>21</sup>. Notably, numerous living organisms deploy surface microstructures to control friction without lubricants <sup>22</sup>. The shapes and sizes of these microstructures differ, such as firebrats (submicron-sized wrinkle structures) 23 and crickets (hexagonal micropatterns) <sup>24</sup>. However, the details of their hierarchical structure remain unclear. Necrophila japonica also lives in an environment where its back contacts various objects, and its hierarchical structure is similar to that obtained by

combining a firebrat and cricket; therefore, the surface microstructure of its back may be involved in friction.

In general dry friction, the frictional force depends on the real contact area rather than the apparent contact area, and the real contact area increases in proportion to the load because the surface roughness deform in proportion to the load. Nevertheless, numerous recent reports indicate that microstructures reduce frictional force due to reduction of contact area <sup>25–28</sup>. In previous study, it was revealed that the apparent contact area could almost be the same as the real contact area in the microscopic region of the microstructure tip as the contact is limited to a small area of the structure tip on a submicron-scale structured surfaces 29 (microcontact). For friction to be proportional to the load on a microcontact surface, the surface microstructure must deform proportionally to the load. Conversely, as shown by arched bridges and submicron-scale metamaterials, certain structural geometries can suppress deformation by dispersing the load across the sides and bottom rather than the surface, thereby avoiding the stress concentrations required for deformation<sup>30–32</sup>. Therefore, the real contact area does not increase proportionally to the load on a surface with a microstructure, and the friction force is expected to be reduced compared to a surface without a structure that follows the Amontn-Coulomb law. In addition, in a single-layer structure, reducing the number of contact points in order to reduce friction leads to pressure concentration, but a hierarchical structure ,e.g., Necrophila japonica reduces the number of contact points while dispersing the load widely across the wrinkles and the dome layer below, improving the deformation suppression effect and potentially reducing friction more than a single-layer structure.

Owing to the complexity involved in directly testing the frictional properties of the body surface of *Necrophila japonica*, we combined the breath figure method <sup>33</sup> with a wrinkle fabrication technique <sup>34,35</sup> to prepare a hierarchical structure,

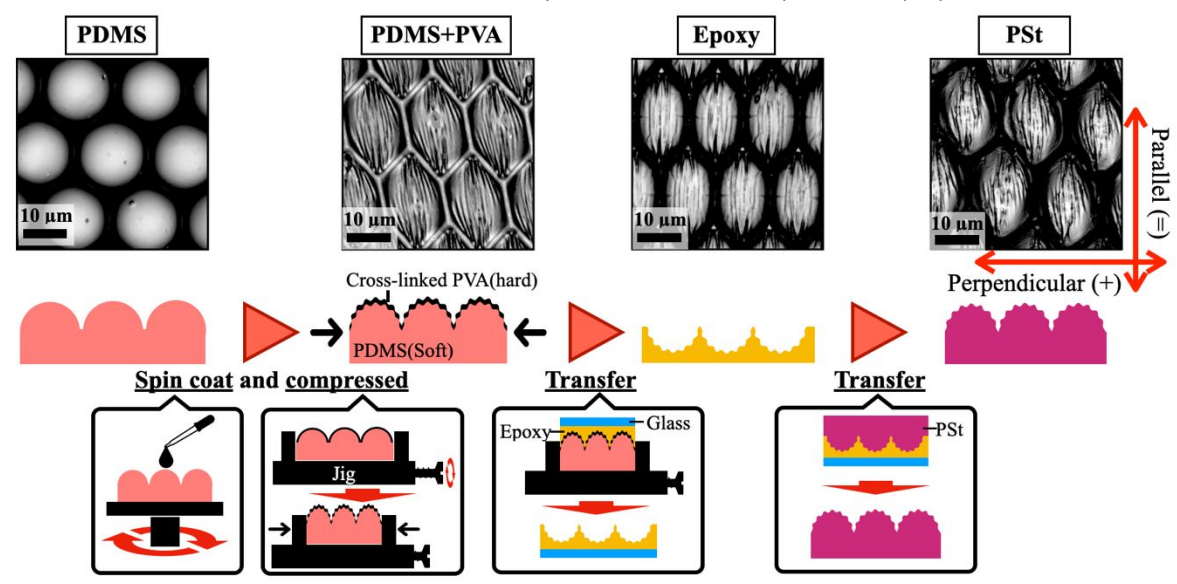


Figure 2 Preparation procedure of the polystyrene (PSt) carrion beetle mimicked structures. Wrinkles were formed by preparing a hard PVA layer on soft PDMS MLAs and compressing it. Although the PVA layer has a large effect on friction, preparing a mimicked structure in a single material using two transfers allows us to investigate the effect of microstructure on friction. Insert images were the laser microscope images of each samples.

which was transferred to prepare a single-material hierarchical mimicked structure using plastic deformation materials. The effect of the hierarchical surface microstructure on friction was investigated by friction force tests on the mimicked structure. The results indicated that the frictional force of hierarchical microstructures exhibiting wrinkle structures on top of microdomes was smaller than that of surfaces without structures, wrinkle-only surfaces, and dome-only surfaces. Thereafter, we analyzed the principle of friction reduction by finite element method (FEM) simulation. The hierarchical structure had a smaller contact area than the other structures, and pressure was concentrated at the tip of the structure. However, hierarchical load dispersion occurred, in which stress was dispersed to the upper wrinkle and dome structures, and the contact pressure was reduced compared to the other structures. Therefore, the hierarchical structure reduced the frictional force by controlling the real contact area by decreasing the contact points and deformation.

#### **Results**

# Preparation of structures mimicking the carrion beetle elytra surface and their friction force measurements

Figure 2 shows the procedure for preparing the mimicked structure. A 2 wt% aqueous solution of polyvinyl alcohol (PVA) was cross-linked by ORGATIX spin-coated polydimethylsiloxane (PDMS) microlens array (MLAs) structures (diameter: 11  $\mu$ m) prepared by the breath figure method <sup>33</sup>. The spin coating was performed at 500 rpm for 5 s and 2000 rpm for 5 s, respectively. To dry and adhere the samples, they were heated in an oven for 12 h at 70°C, after which they were compressed by 20% using a jig and transferred to an epoxy resin and polystyrene (PSt) to prepare a mimicked structure using a single plastic deformation material. To clarify the effect of the microstructure shape on friction, surfaces with wrinkle-only structures and only microlens arrays (MLAs) were prepared. The wrinkled structure was prepared by spin-coating flat PDMS with 1 wt% cross-linked PVA aqueous solution at 500 rpm for 5 s and 3000 rpm for 40 s, compressing with a jig, and transferring to an epoxy resin and PSt (Figure S3). The MLAs structures were prepared by compressing the symmetrical PDMS-MLAs structure of the template with a jig and transferring it two times in the same manner (Figure S4). The prepared samples were observed and their sizes were measured using a laser microscope. The prepared structures exhibited the following size: wrinkle (1.39  $\pm$  0.31  $\mu m$  diameter, 0.32  $\pm$  0.13  $\mu m$  depth) and MLAs (12.10  $\pm$  0.68 × 9.80  $\pm$  0.29  $\mu m$  diameter, 1.73  $\mu m$   $\pm$ 0.31 depth); the mimic structure exhibited a combined size (wrinkle:  $1.38\pm0.33$  µm, MLAs:  $12.23\pm0.47\times9.77\pm0.33$  µm). The size was the mean value (n=20) for any structure and the number after ± was the standard deviation.

The frictional force of the samples was measured by sliding the samples with a 9.8 mN load in one direction using a friction tester. To investigate the effect of an anisotropic structure on friction, the measurement direction was distinguished between the perpendicular (+) direction, which crossed the structure, and the parallel (=) direction, which was parallel to the structure

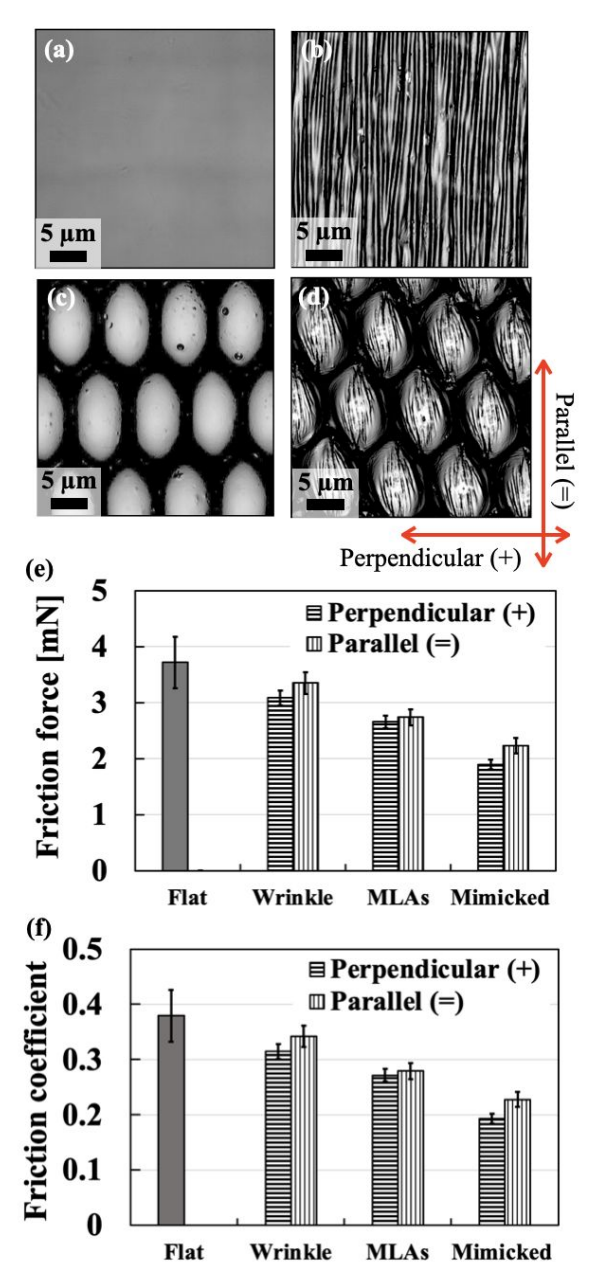


Figure 3 (a-d) The laser microscope images, (e) the frictional force and (f) friction coefficient of (a) flat, (b) wrinkle, (c) MLAs, and (d) carrion beetle mimicked structure. Load was 9.8 mN. The friction coefficient was calculated from each dynamic friction force and load, and the dynamic friction force was the average of the friction forces at 1000-5000 ms. Red arrows show sliding direction (+; perpendicular, =; parallel). All error bar were standard deviation.

(Figure 3). The measured frictional force and friction coefficient are shown in Figures 3(e, f). The friction force varied greatly with the shape of the microstructure, decreasing in the flat > wrinkle > MLAs > mimicked structure order regardless of the sliding direction, and the friction force on the mimicked structure surface was approximately~50% lower than that on the flat surface with no microstructure. These results indicated that the mimicked structure exerted a friction-reducing effect that is greater than that exerted by a single-layer structure. Additionally, the frictional force of samples other than the flat

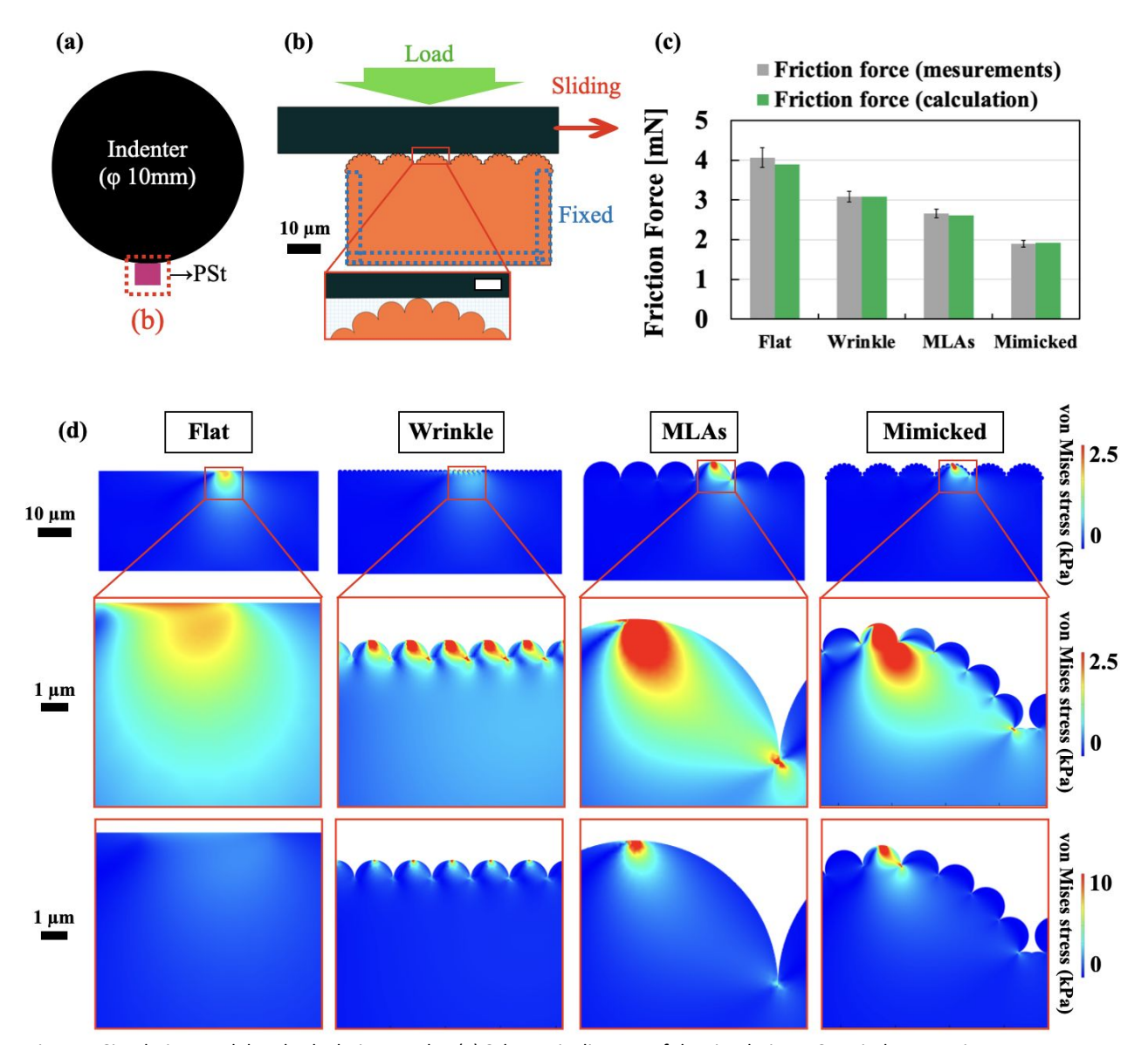


Figure 4 Simulation model and calculation results. (a) Schematic diagram of the simulation. PSt to indenter ratio was not accurate. (b) Simulation model of mimicked structure. Insert image was magnified image. Only a portion of the indenter was shown. White scale bar was 1.4 µm. (c) Calculation and measurements results of friction force. (d) Simulation results showing deformation stress applied during sliding. The indenter was omitted. The top row were an overall view, and the bottom two rows surrounded by a red frame were magnified views. The two magnified images had different scale bar ranges, with the upper one being up to 2.5 kPa and the lower one being 10 kPa (see left side of the figure). On the right side of the images were a scale bar that shows the size of each row. All error bar were standard deviation.

structure was investigated by changing the sliding direction, revealing that the frictional forces of the wrinkle, MLAs, and mimicked structure were smaller in the perpendicular direction than in the parallel direction. The anisotropies of the frictional force in different sliding directions could be caused due to stiction length and stiffness, as revealed in previous studies <sup>36</sup>. The paper shows that when the structure size is less than 10e-3 of the indenter size, the anisotropy due to the stiction length becomes more pronounced, and our paper has the same scale ratio, since the b/R in the original paper is around 10e-4 to 10e-3. The microstructures in this study that exhibited anisotropy in frictional forces also had shorter stiction lengths because contacts perpendicular to the microstructure are shorter than

contacts parallel to the microstructure. The stiffness, which is inversely proportional to the surface deformation, may be explained by the load dispersion that will be discussed later in the text. That is, different shapes have different deformation resistances and therefore different frictional forces. Of the two, the stiction length was similar to the difference in contact continuity that explains the anisotropy of friction forces in metal surface microstructures<sup>27</sup>.

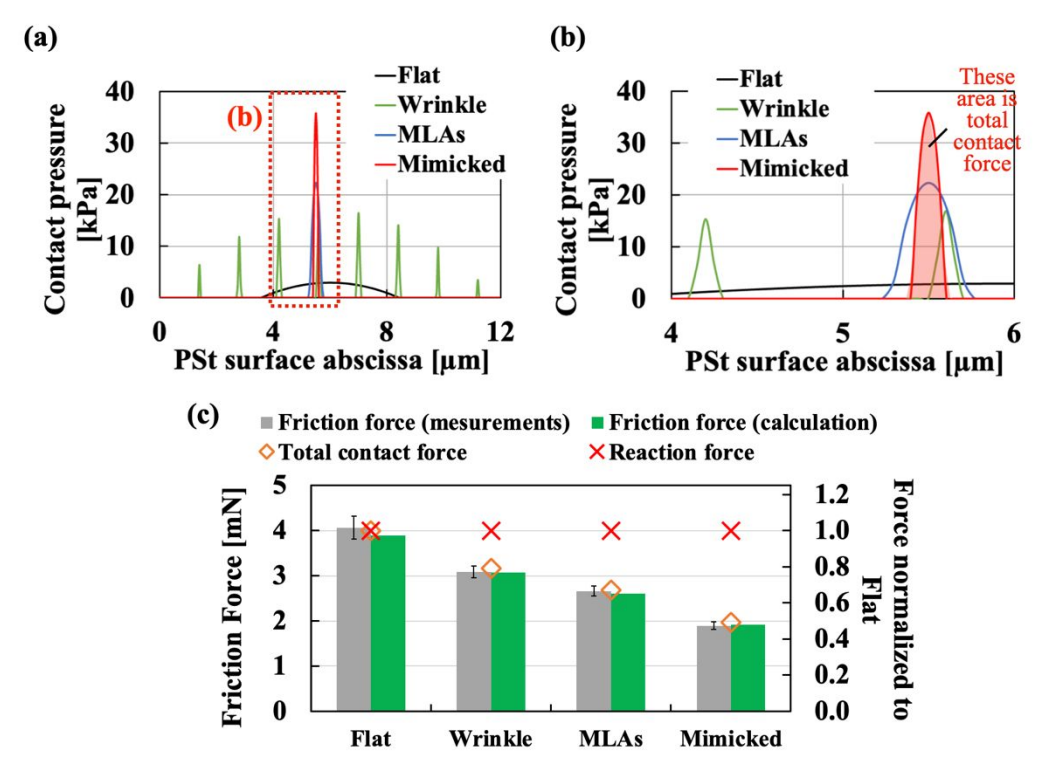


Figure 5 (a) Contact pressure during sliding (when the tip of the indenter was at 6 μm on the horizontal axis of the graph) and (c) measured and calculated friction force results (left vertical axis) and ratio of contact force pressure and reaction force to flat (right vertical axis). The contact force and reaction force are normalized to the flat value. (a, b) The horizontal axis of the graph was the coordinate, and 0 μm was the center position of the PSt model. (b) was an magnified view of (a) (the area surrounded by the red dot shown in (a)). Total contact force pressure was the area of pressure applied to the surface as shown in (b). The reaction force was the total force applied to the PSt model as shown in Figure 4 (d). All error bar were standard deviation.

## Consideration of friction reduction factors by FEM simulation

A simplified friction model was considered to investigate the friction reduction of the hierarchical structure. In this model, the frictional force was obtained by the product of the contact pressure generated by the virtual spring inserted at the interface and the friction constant. Put differently, the calculation was based on Coulomb's law, which considers the real contact area, which varies proportionally to the load, rather than the apparent contact area <sup>37</sup>. The indenter of the same size as in the actual measurement was placed on top of the modeled microstructure sample used for the actual measurement (Figures 4 and S5). Figure 4 (b) shows a magnified image of one part of the indenter and the PSt model. The frictional force, stress, and contact pressure applied to the PSt model when the indenter was slid laterally with a 9.8 mN load were calculated.

The calculated frictional force is shown in Figure 4 (c) and S5 (i). The calculated frictional force correlated well with the actual measured frictional force, decreasing in the flat > wrinkle > MLAs > Mimicked order. The frictional force in this calculation was determined by the product of the friction constant and contact pressure applied to the indenter and the model interface. As the friction constant was set to the same value for all structures, the applied pressure to the model have changed by the surface microstructure. Figure 4 (d) shows the results of the calculation of the deformation stress applied during sliding.

A larger stress concentration was observed at the tip of the structure compared with the flat surface owing to the microstructure. In the flat model, stress attenuates in proportion to the distance. However, in the model exhibiting a surface microstructure, significant stress was applied to the base of the structure far from the contact point. Particularly, the mimicked structure exhibited widely dispersed stresses in the upper wrinkled structure and lower MLAs structure. This difference in stress dispersion may indicate that the forces acting on the surface, which are prone to deformation due to pressure concentration, have changed depending on the structure.-Figures 5 (a, b) show the applied contact pressure to the interface during sliding (at 14 µm from the initiation of sliding). The abscissa shows the coordinate of the PSt model surface. The PSt model was set up so that the center of the PSt model was at 0. The applied contact pressure by each structure was different, with the flat structure having the lowest maximum value, followed by the wrinkle and MLAs structures; the mimicked structure having the highest maximum value. Contrarily, the stress range was smallest for the mimicked structure and increased in the following order: MLAs < wrinkle < flat. If the total value of this contact pressure (the colored part in Figure 5 (b)) was not changed based on the structure, the frictional force would be unchanged. However, force calculations normalizing the total contact pressure on the surface to the flat revealed a different ratio on the shape of the structure even when the same load was applied (Figure 5 (c),

total contact force). The total contact force decreased in the following order: flat > wrinkle > MLAs > mimicked, similar to the actual measured and calculated friction force results, and the ratio-of decrease corresponded well with the amount of decrease in friction force. Conversely, in contrast to the contact force, which looked at the force applied only to the interface, the reaction force applied to the entire PSt model was constant regardless of the structure; therefore, the structure may have reduced the applied force to the surface by dispersing the force to locations other than the surface (Figure 5 (c), reaction force rate). Differences were observed in the stress distribution based on the structure (Figure 4(d)). Stress dispersion to the bottom and sides of the structure avoids stress concentration on contact surfaces where deformation tends to occur. As a result, it is harder for the material to reach the stress required for deformation, which is thought to suppress deformation and real contact area increase and reduce friction.

#### Discussion

The above results indicated that hierarchical surface microstructures mimicking Necrophila japonica, do not exhibit superhydrophobicity, although they improved wettability (Figure S2) and significantly reduced friction compared with flat and single-layer microstructure surfaces. The friction-reduction effect by the mimicked structure can be probably explained by the load-dispersion effect. There are many factors that affect friction force, but in dry friction such as the one we conducted, it has been reported that the adhesive force acting on the real contact area between the indenter and the friction surface has a large effect on the friction force<sup>25</sup>. In the case of the contact between hard plastic deformation materials, the real contact area is extremely small compared with the apparent contact area owing to the influence of roughness on the surfaces. When the load is increased, pressure is concentrated on the roughness and deformation increases the real contact area and frictional force  $^{38-40}$ . In other words, the deformation of the roughness in proportion to the load is the basis of normal friction. Conversely, the simulations revealed that the microstructure reduced the contact area and concentrated the pressure at the tip of the structure. The decrease in the contact area was related to the structure shape, with the area where the mimicked structure contacted the indenter being the narrowest and the pressure applied to the model surface being the highest (Figures 4 (d) and Figure 5 (a, b)). In such a case, the apparent and real contact areas may almost be the same at the tip of the microstructure 29 (microcontact). Artificial and natural rough surfaces of comparable dimensions to the surface structures substantially reduce the frictional force on the surface in contact with the insect legs <sup>29,41</sup>. Gorb et al. suggest that this reduction in frictional force is due to a decrease in the real contact area, which can be calculated as the sum of distances between all virtual contact points on the nondeformable terminal plate and substrate29. Indeed, the observed trends in calculated and measured values align consistently, underscoring the significant variation in frictional force contingent upon structure size<sup>29</sup>. From these results, it is apparent that contact on the surface of the surface

microstructure is primarily concentrated at the tip, where the apparent and real contact areas are nearly identical. According to the Amonton-Coulomb law, even after microcontact, the frictional force will not change with the structure if the real contact area increases owing to the deformation of the microstructure. However, in the actual and simulated measurements, the frictional forces decreased by the microstructure (Figure 4(c)). Notably, although the reaction force, which is the force applied to the entire model, was the same for all structural models, the contact force applied to the structure-indenter interface decreased with flat, wrinkle, MLAs, and mimicked, as did the friction force(Figure 5(c)). Despite applying the same load, the fact that the total contact force applied to the surface prone to stress concentration was small indicated that deformation and increase in real contact area was difficult to occur on the actual surface. The reason for the decrease in contact pressure was that the load was dispersed to areas other than the surface, as seen in bridges and metamaterials. In a sample exhibiting a microstructure, the stress was dispersed to the roots of the structure without attenuation proportional to distance, which reduced the contact pressure (Figure 4 (d)). Additionally, although the stresses in the wrinkle and MLAs structures were dispersed within and at the root of each structure, the stresses in the hierarchical mimicked structure were widely dispersed in the upper wrinkle structure and lower MLAs structure(Figure 4 (d)). In addition, the mimicked structure exhibited the lowest contact pressure and friction force (Figure 5 (c)). For the above reasons, the mimicked structure had the strongest pressure concentration due to the reduction in contact points (Figure 5 (a, b)), but the frictional force decreased the most with the difference in apparent contact area because the deformation (large increase in real contact area) was suppressed by effective load dispersion. Although the conditions in our study are significantly different, these results are similar to those of studies showing behavior that differs from the Amontton-Coulomb law in under low load conditions where even plastic deformation materials only undergo elastic deformation<sup>42</sup>. The region where deformation is difficult can be extended by the surface microstructure, and this may be more effective with a hierarchical structure than with a single layer structure. In our case, the indenter was sufficiently large in relation to the size of the structure to reduce the frictional force due to the simple reduction of the contact points. If the indenter and microstructure sizes were closer, the frictional force may increase owing to the interlock caused by the penetration of the structures by the indenter <sup>25,26,43</sup>. Conversely, if the hierarchical structure was used, the contact point might be lowered without increasing the gap to penetrate. The friction reduction effect was also confirmed in a random-sized model that was close to the actual mimicked structure, so the impact of non-uniformity in the structure was small (Figure S6).

Based on these results, the microstructure placed on the dorsal surface of the carrion beetle might reduce the energy loss due to friction during movement on friction-prone forest surfaces, such as under fallen leaves. Additionally, such a hierarchical structure exists in the *Necrophila japonica* as well

as springtails 13,20 and slithering geckos 21, each of which share the same habitat on the ground surface and in the soil environment. Although the hierarchical structure, such as a lotus leaf <sup>22</sup> and slithering gecko <sup>21</sup>, may be effective in reducing friction, detailed studies have not been conducted. Several studies have investigated friction in hierarchical structures inspired by snake scales, although they did not consider the effects of the structure itself because it did not comprise a single material like ours 44. Additionally, the utilized material is an elastic deformation material that has a different friction principle from the plastic deformation material we investigated here. A snake scale-inspired material made of plastic deformation material exhibits a friction-reduction effect of ~40%; however, it is a single-layer structure 25. The frictionreducing effects of various other structures have been investigated, although most were single-layer structures <sup>26,27</sup>. Alternatively, lubricants were used or mixed with different materials<sup>45–47</sup>. In terms of dry friction reduction due to surface microstructures, there has been much discussion about the reduction in contact area, as expressed by the Hertz contact theory due to the microcontact state. However, there has been little discussion about deformation due to the pressure concentrated on the reduced contact area, which we explained by incorporating knowledge from the field of structural geology. Thus, the result that hierarchical structures are advantageous in reducing friction may allow for feedback into biology. Anisotropic structures also exhibit anisotropy in frictional forces <sup>25,48,49</sup>, which could result in survival strategies by restricting or selecting the movement direction. Compared with previous studies <sup>36</sup>, the structure geometry differs depending on the sliding direction, which may affect the stiction length and stiffness. The stiction length had the same microstructure and indenter scale ratio as ours. In particular, for stiffness, the authors used the penalty method as we did to show the difference between the force acting on the entire surface and the force acting on the surface. Therefore, the anisotropy of the structure may also affect the load dispersion effect. Frictional anisotropy due to structural anisotropy is also demonstrated by snakes. The sizes of these microstructures exhibiting anisotropy are on the submicron scale similar to the wrinkle structure of the Necrophila japonica <sup>25,48,49</sup>. Further studies are desired to elucidate the effects of structure on anisotropy as well as their behavioral patterns of carrion beetle, and we anticipate further progress. Additionally, our results can be applied to various fields, such as architecture, medicine, and industry. Considering future applications for human society, it is advantageous to be able to reduce friction without using lubricating oil, which causes environmental pollution and other issues 50. Another important environmental consideration is the use of selforganization to prepare mimicked structures, as in living organisms, rather than lithography or etching, which require cost, time, and special equipment 51-55.

#### **Conclusions**

In conclusion, our research has for the first time uncovered the wettability enhancement and friction reduction function of the hierarchical surface microstructure of *Necrophila japonica*.

By combining knowledge from the field of structural mechanics that structural shape affects deformation with basic principles of friction, we have newly revealed-that the friction properties and mechanisms of the hierarchical surface microstructures. The hierarchical surface microstructure of Necrophila japonica reduces friction more than the monolayer structure because the reduction in contact points and the effective hierarchical load dispersion effect suppress the deformation and the increase in real contact area. This will lead to elucidation of the microstructural functions of many organisms, not just the carrion beetle, and will provide useful knowledge for reducing friction without lubrication in human society. Our research is environmentally friendly, not only because we do not use lubricants, but also because we can create mimicked structures in the same environmentally benign way as living organisms, through self-organization. Our research, focusing on living organisms, allows us to find new connections between findings from different fields: friction reduction and load dispersion. In the metamaterial field, excellent load-bearing properties attributed to various complex hierarchical structures have been reported 31,32,56, and if more systematic studies are conducted, more freedom regarding friction design (anisotropy and selective expression of required friction force) is expected by selecting the necessary size, shape, and material for controlling friction.

#### **Experimental section**

#### Preparation of the reverse microstructures

This section describes the method for preparing the mold used for the measurements. (Figures 2, S3, and S4). The polyvinyl alcohol (PVA, FUJIFILM Wako Pure Chemical Corporation, Japan) cross-linked with an ORGATIX (TC315, Matsumoto Fine Chemical Co. Ltd, Japan) solution was prepared by mixing both solutions with a magnetic stirrer overnight so that the mixing ratio of PVA (hydroxyl group) to ORGATIX (carboxyl group) was 1:1. To prepare the wrinkle structure, a 1 wt% PVA aqueous solution was dropped on flat polydimethylsiloxane (PDMS, crosslinking ratio = base agent:curing agent = 10:1, DOWSILTM, SILPOT 184 W/C, DuPont Toray Specialty Materials K.K., Japan) without a structure and spin-coated. First, the solution was spread by spin coating at 500 rpm for 5 s, after which the thickness was adjusted by spin coating at 3000 rpm for 40 s (Figure S3). To prepare the mimicked structure, a 2 wt% PVA aqueous solution was dropped onto the PDMS-MLAs and spin-coated at 500 rpm for 5 s, followed by 2000 rpm for 5 s (Figure 2). The solution concentrations and spin-coating conditions for the wrinkled and mimicked structures differed because, in the case of MLAs, the liquid easily escapes owing to the microstructure, which is similar to a frog adhesive toe pad <sup>57</sup>. The spin-coated samples were dried in an oven at 70°C for 12 h to improve adhesion. Next, the PVA/PDMS sample was compressed by 20% using a hand-operated device (X-Axis, Left/Right Screw, Open/Close Width Adjusting Units, XANON60, MISUMI Corporation, Japan) for the precise control of PDMS compression. Finally, an epoxy resin (Epok 812, Okenshoji Co., Ltd, Japan) was dropped onto the 20% compressed sample, covered with a cleaned glass

substrate, and heated at 60°C for 12 h to transfer the structure to the epoxy resin. The MLAs structure employed for the friction measurements was prepared by compressing the symmetric MLAs structure in a mold with a jig without spin coating, followed by transferring it to the epoxy resin (Figure S4).

#### Preparation of the polystyrene microstructure

The PSt sample was prepared by dropping a PSt chloroform solution (100 g/L) onto an epoxy resin mold with the structure prepared in the same manner as that employed for the preparation of the reverse microstructures: letting it air dry and peeling it off (Figures 2, S3, and S4). The flat samples were prepared by dropping the solution onto a glass substrate and peeling it off after natural drying. The structures of the prepared samples were observed and measured (n = 20) by a laser microscope (VK-X200, Keyence Corp., Japan)

#### Measurements of the water contact angle

The water contact angle (WCA) of the sample surface was measured by a contact-angle analyzer (FAMAS, Drop Master, Kyowa Interface Science, Japan). The static WCA of the elytra of the carrion beetle was measured at 1  $\mu L$ , and the static WCA of the PSt sample surface was measured by dropping 3  $\mu L$  of ultrapure water onto the sample surface. The contact angle was distinguished based on whether it was perpendicular or parallel to the wrinkle structure (Figure S2(c)). Perpendicular (+) was used to observe the water droplets in the perpendicular direction, and parallel (=) was used to observe the water droplets in the parallel direction. The average value of six measurements was taken for the elytra of the carrion beetle, and the average value of four measurements was taken for the PSt sample. The error bars in the graph represent the standard deviation.

#### Measurements of friction force

The frictional force of the sample was measured by sliding the sample in one direction with a constant load using TRIBOGEA (HHS2000, SINTO Scientific Co., Ltd., Japan). The employed indenter was a stainless steel ball (SUS304, AS ONE Corporation, Japan) with a 10 mm diameter (Ra = 32.7 nm). The sliding speed for the friction measurement was 1 mm/s, and the load was 9.8 mN (≒1 g). The friction measurements were performed four times per sample, and the average frictional force was calculated for measurement times ranging from 1000 to 5000 ms ( $\mu m$ ). The measurement directions were divided into two types: those measured in the direction across the wrinkles or MLAs (perpendicular, +), and those measured in the direction parallel to the structure (parallel, =). This difference in the sliding direction did not apply to flat surfaces, and unless otherwise specified, the sliding direction was perpendicular. All error bars in the graph represented the standard deviation.

## Finite element method simulation of the friction properties

Finite element method (FEM) simulations were performed using COMSOL Multiphysics with the structural mechanics module (COMSOL Multiphysics 6.1, COMSOL Inc., USA) running on Windows 10 Pro (Ver. 1909). The mimicked-structure

model was prepared by arranging hemispheres (diameter: 11 μm) in a row horizontally on a rectangle as an MLAs structure, and with hemispheres (diameter: 1.4 µm) arranged as a wrinkled structure on the circumference of the MLAs (Figure S5(d)). The MLAs structure was prepared by arranging only 11 µm diameter hemispheres in a rectangular pattern (Figure S5(c)), and the wrinkle structure was prepared by arranging only 1.4 µm diameter hemispheres in a rectangular pattern (Figure S5 (b)). The rectangle and hemisphere corresponding to the PSt parts were all integrated, leaving no interface. The rectangle and hemisphere that corresponded to the PSt parts were completely combined (union). The flat structure does not have hemispheres lined up but consists only of rectangles (Figure S5 (a)). The thickness and width of the rectangle were 30 and 66 µm, respectively, but the wrinkle structure was set to 65.8 µm to avoid differences in calculations owing to gaps and edges without structures (47 hemispheres with a diameter of 1.4  $\mu m$  are arranged without any gaps, and it has been confirmed that this size difference exerted almost no effect). Considering the influence of curvature, the indenter was set to 10 mm, the same as the actual indenter, and only a portion was cut out or hidden when displaying the results and model (Figures 4(a, b)). The indenter was placed 10  $\mu m$  to the left from the center of the PSt structural model and adjusted vertically so that the lower apex of the indenter and upper apex of the structural model were at the same height. The material properties of the stainless steel indenter and structural model were obtained from the COMSOL material library, and the calculation mesh size was adjusted to suit the calculation. The mesh model is shown in Figures S5 (e-h). The contact model in COMSOL was used as a model for calculating the frictional force generated at the indenter and structure interface. This model defined the contact by inserting a very thin spring at the interface. In this method, the frictional force was calculated in a simplified manner using the product of the contact pressure generated by the interface spring and the friction constant (constant). Put differently, the focus was not on the apparent contact area; rather, it was on the real contact area, which varied depending on the load and adhesive force generated at the interface. Therefore, the calculation was based on the Coulomb law <sup>37</sup>. The parameters in the contact model were entered with values that were adjusted to ensure accurate calculations(Contact pressure penalty factor (P<sub>n</sub>): 5e3 [N/mm<sup>3</sup>], Friction force penalty factor ( $f_t$ ): 0.01 (Automatic, Soft), Spring foundation ( $k_{tot}$ ): 7e5 [N/m]). The penalty method was chosen for the contact model. The frictional force was calculated by fixing one part of the model to ensure correct calculations, applying a load from the top of the indenter, and sliding the indenter 20  $\mu m$  laterally (Figure 4(b)). A spring foundation was used for fixing the indenter to stabilize the calculations. The frictional force displayed in the graph is the average value of the obtained frictional force. The calculated friction was the steady state friction. The contact force in the graph was calculated by summing all contact pressures applied to the structure surface during sliding. The contact force and reaction force (y component) are normalized to the flat value. (so the ratio of flat is 1). In other words, the

4

7

contact force is the product of the contact pressure and the contact area. The contact pressure and stress during sliding, which were not total values, were shown at a sliding distance of 14  $\mu m$ .

#### **Author contributions**

K.T. conceived the idea for the study and Y.H. and Y.M. supported it. K.T. collected the carrion beetles and observed them with FE-SEM. K.T. designed, prepared, and measured all friction samples. K.T. designed the all models and performed the FEM simulations. K.T. visualized the obtained data. Y. H. provided support for measurements, including the provision of a friction tester. Y.M. provided the simulation software and provided overall supervision. K.T. and Y.H. acquired the funding, and Y.M. provided the laboratory space and supplies. K.T. wrote the manuscript. M.S. and the other authors reviewed drafts of the manuscript and revised it critically for intellectual content. All authors approved the final version of the manuscript for publication.

#### Conflicts of interest

There are no conflicts to declare.

#### Data availability

The authors confirm that the data supporting the findings of this study are available within the article and its supplementary materials.

#### **Acknowledgements**

A part of this work was supported by "Advanced Research Infrastructure for Materials and Nanotechnology in Japan (ARIM)" of the Ministry of Education, Culture, Sports, Science and Technology (MEXT). Grant Number JPMXP1223HK0073 and Open Facility, Global Facility Center, Creative Research Institution, Hokkaido University.

This work was supported by the Research Program for CORE lab under the cooperative research program of "NJRC Mater. & Dev. (MEXT)" Grant 20236001, JST SPRING, Grant Number JPMJSP2119, and Grant-in-Aid for JSPS Fellows, Grand Number 24KJ0256.

#### **Notes and references**

‡ Footnotes relating to the main text should appear here. These might include comments relevant not central to the matter under discussion, limited experimental and spectral data, and crystallographic data.

§ §§ etc.

L. Chambers, P. Roach and N. Shirtcliffe, Surf Innov, 2022,
 10, 341–372.

- W. Krings, D. Konn-Vetterlein, B. Hausdorf and S. N. Gorb, *Front Zool*, 2023, **20**, 37.
- 3 C. G. Bernhard, G. Gemne and J. Sällström, *Z. vergl. Physiologic*, 1970, **67**, 1–25.
  - J. Cai and L. Qi, *Mater Horiz*, 2015, **2**, 37–53.
- 5 X. Wang, D. Tan, X. Zhang, Y. Lei and L. Xue, *Biomimetics*, 2017, 2, 10.
- 6 T. Endlein and W. Federle, *PLoS One*, 2015, **10**, e0141269.
  - W. Jiang, B. Lei, H. Liu, D. Niu, T. Zhao, B. Chen, L. Yin, Y. Shi and X. Liu, *Nanoscale*, 2017, **9**, 2172–2177.
- 8 K. Tsujioka, Y. Matsuo, M. Shimomura and Y. Hirai, *Langmuir*, 2022, **38**, 1215–1222.
- J. Li, C. Ma, J. Liu, X. Dong and J. Liu, *Biosurf Biotribol*, 2021,
   7, 180–186.
- Y. Watahiki and K. Sasakawa, *Entomol Exp Appl*, 2019, **167**, 85–90.
- 11 H. Ikeda and T. Sota, *Ecol Evol*, 2011, **1**, 97–105.
- H. Ikeda, T. Kagaya, K. Kubota and T. Abe, Evolution (N Y), 2008, 62, 2065–2079.
- 13 R. Helbig, J. Nickerl, C. Neinhuis and C. Werner, *PLoS One*, 2011, **6**, e25105.
- 14 K. Koch, B. Bhushan and W. Barthlott, *Prog Mater Sci*, 2009, 54, 137–178.
- S. Parvate, P. Dixit and S. Chattopadhyay, *Journal of Physical Chemistry B*, 2020, 124, 1323–1360.
- 16 Y. He, L. Wang, T. Wu, Z. Wu, Y. Chen and K. Yin, Nanoscale, 2022, 14, 9392–9400.
- G. D. Bixler and B. Bhushan, *Nanoscale*, 2013, 5, 7685–7710.
- 18 B. Bhushan, *Philosophical Transactions of the Royal Society A: Mathematical, Physical and Engineering Sciences*, 2009, **367**, 1445–1486.
- 19 B. Su, Y. Tian and L. Jiang, J Am Chem Soc, 2016, 138, 1727– 1748
- R. Hensel, R. Helbig, S. Aland, A. Voigt, C. Neinhuis and C. Werner, NPG Asia Mater, 2013, 5, e37.
- 21 M. Spinner, S. N. Gorb and G. Westhoff, *Proceedings of the Royal Society B: Biological Sciences*, 2013, **280**, 20132160.
- 22 H. A. Abdel-Aal, Surf Topogr, 2016, 4, 043001.
- Y. Hirai, N. Okuda, N. Saito, T. Ogawa, R. Machida, S. Nomura, M. Ôhara, M. Haseyama and M. Shimomura, *Biomimetics*, 2019, **4**, 2.
- 24 M. Varenberg and S. N. Gorb, *Advanced Materials*, 2009, **21**, 483–486.
- 25 M. J. Baum, L. Heepe, E. Fadeeva and S. N. Gorb, *Beilstein Journal of Nanotechnology*, 2014, 5, 1091–1103.
- N. Li, E. Xu, Z. Liu, X. Wang and L. Liu, Sci Rep, 2016, 6, 39388.
- Y. Shimada, K. Tsujioka, Y. Matsuo, M. Shimomura and Y. Hirai, Molecular Crystals and Liquid Crystals, 2024, 768, 158–167
- 28 M. Nosaka, K. Tsujioka, Y. Matsuo, T. Okamatsu, T. Arita, M. Shimomura and Y. Hirai, *Langmuir*, 2021, 37, 6459–6467.
- D. Voigt, J. M. Schuppert, S. Dattinger and S. N. Gorb, J Insect Physiol, 2008, 54, 765–776.
- F. Trentadue, A. Fiore, R. Greco, G. C. Marano and N. D. Lagaros, *Front Built Environ*, 2020, **6**, 74.
- L. R. Meza, A. J. Zelhofer, N. Clarke, A. J. Mateos, D. M. Kochmann and J. R. Greer, *Proc Natl Acad Sci U S A*, 2015, 112, 11502–11507.

- J. Bauer, S. Hengsbach, I. Tesari, R. Schwaiger and O. Kraft, Proc Natl Acad Sci U S A, 2014, 111, 2453–2458.
- 33 H. Yabu, Sci Technol Adv Mater, 2018, 19, 802–822.
- 34 L. Ma, L. He and Y. Ni, J Appl Phys, 2020, **127**, 111101.
- M. Nania, O. K. Matar and J. T. Cabral, Soft Matter, 2015,
   11, 3067–3075.
- 36 C. Yu, H. Yu, G. Liu, W. Chen, B. He and Q. J. Wang, *Tribol Lett*, 2014, **53**, 145–156.
- 37 CONSTITUTIVE MODEL FOR FRICTION
  https://doc.comsol.com/6.1/doc/com.comsol.help.sme/sm
  e ug theory.06.083.html#4026583, (accessed July 2024).
- 38 F. P. Bowden and D. Tabor, *Proceedings of the Royal Society of London*, 1939, **169**, 391–413.
- 39 J. F. Archard, Proceedings of the Royal Society of London, 1957, 243, 190–205.
- 40 J. A. Greenwood and J. B. P. Williamson, *Proceedings of the Royal Society of London*, 1966, **295**, 300–319.
- 41 E. V. Gorb and S. N. Gorb, *J Exp Bot*, 2017, **68**, 5323–5337.
- 42 M. Tajdari and M. Javadi, J Mater Process Technol, 2006, 177. 247–250.
- I. H. Sung, H. S. Lee and D. E. Kim, Wear, 2003, 254, 1019– 1031.
- 44 M. Wang, S. K. Ghosh, C. M. Stafford, A. K. Blevins, S. Huang, J. Martinez, R. Long, C. N. Bowman, J. P. Killgore, M. Zou and Y. Ding, ACS Appl Mater Interfaces, 2020, 12, 57450–57460.
- D. Li, Z. Wang, D. Wu, G. Han and Z. Guo, *Nanoscale*, 2019,
   11, 11774–11781.
- 46 S. K. Sinha, N. S. Seh and C. Lim, *Nano-tribology and Materials in MEMS*, Springer Berlin, Berlin, 1st edn., 2013.
- J. Ma, Y. Liu, J. Mostaghimi and N. Zhang, *Tribol Int*, 2024, 191, 109107.
- 48 R. A. Berthé, G. Westhoff, H. Bleckmann and S. N. Gorb, *J Comp Physiol A Neuroethol Sens Neural Behav Physiol*, 2009, **195**, 311–318.
- 49 H. A. Abdel-Aal, R. Vargiolu, H. Zahouani and M. El Mansori, Wear, 2012, 290–291, 51–60.
- 50 D. Hörner, *Journal of Synthetic Lubrication*, 2002, **18**, 327–347.
- 51 A. Zhang, H. Bai and L. Li, *Chem Rev*, 2015, **115**, 9801–9868.
- 52 J. F. V. Vincent, O. A. Bogatyreva, N. R. Bogatyrev, A. Bowyer and A. K. Pahl, *J R Soc Interface*, 2006, **3**, 471–482.
- 53 M. Shimomura and T. Sawadaishi, *Curr Opin Colloid Interface Sci*, 2001, **6**, 11–16.
- A. Muñoz-Bonilla, M. Fernández-García and J. Rodríguez-Hernández, *Prog Polym Sci*, 2014, **39**, 510–554.
- J. Rodríguez-Hernández, *Prog Polym Sci*, 2015, **42**, 1–41.
- 56 L. Cheng, T. Tang, H. Yang, F. Hao, G. Wu, F. Lyu, Y. Bu, Y. Zhao, Y. Zhao, G. Liu, X. Cheng and J. Lu, Advanced Science, 2021, 8, 2002701.
- W. Federle, W. J. P. Barnes, W. Baumgartner, P. Drechsler and J. M. Smith, *J R Soc Interface*, 2006, **3**, 689–697.

### Data availability statements

# Friction-reduction effect of the hierarchical surface microstructure of carrion beetle by controlling the real contact area

Kazuma Tsujioka,<sup>a</sup> Yuji Hirai,<sup>b</sup> Masatsugu Shimomura<sup>b,c</sup> and Yasutaka Matsuo\*<sup>d</sup>

<sup>a</sup>Graduate School of Chemical Sciences and Engineering, Hokkaido University, N13, W8, Kita-ku, Sapporo 060-8628, Japan.

<sup>b</sup>Graduate school of Science and Technology, Chitose Institute of Science and Technology, Bibi 758-65, Chitose, 066-8655, Japan.

<sup>c</sup>Department of Applied Chemistry and Bioscience, Chitose Institute of Science and Technology, Bibi758-65, Chitose, 066-8655, Japan.

<sup>d</sup>Nanotechnology Research Center, Research Institute for Electronic Science, Hokkaido University, N21W10, Kita-ku, Sapporo, 011- 0021, Japan.

E-mail: matsuo@es.hokudai.ac.jp;

The authors confirm that the data supporting the findings of this study are available within the article and Electronic supplementary information